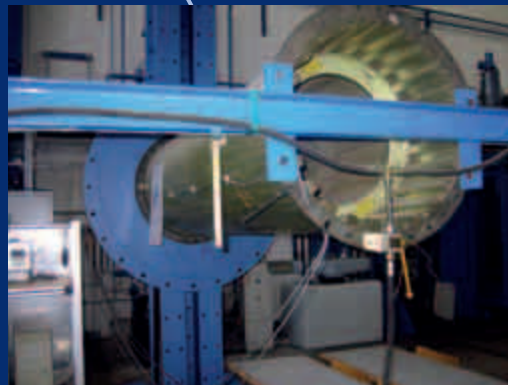


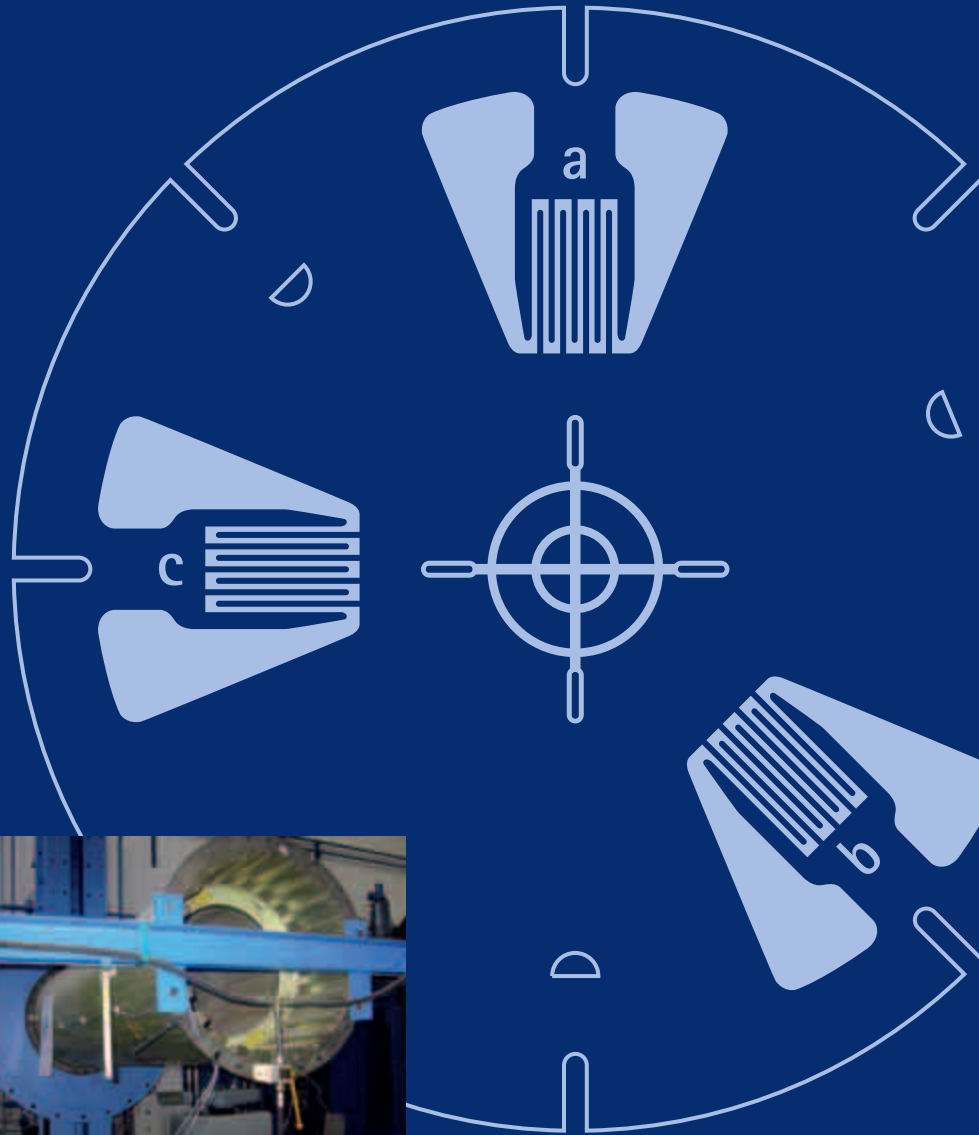
reports in applied measurement



Experimental analysis of mechanical stress in passive reinforcement anchorages in C-C-T nodes



Determination of plain stress using strain gage rosettes





ram reports in applied measurement

Determination of plain stress using strain gage rosettes

Siegmar Tittel, Dresden, Germany

Introduction

In the last decades, strain gage technology has developed into a standard procedure for experimental stress analysis. It is generally the case that three fully independent stress components are fixed on the surface of structural elements, so that three independent quantities, in this case strains, have to be measured in three different directions. This is done with SG rosettes, specifically designed by the manufacturer with directions of measurement relative to one another. Other manufacturers, as well as the traditional SG rosette supplier, Hottinger Baldwin Messtechnik GmbH (HBM), are becoming established in Germany. Each manufacturer has introduced its own company-specific designation for the individual SGs that combine to make up the rosette, whereby not only the SG designation differs (a, b, c, or 1, 2, 3,), but also the angle assignment (for example, 0°, 45°, 90° can correspond to 1, 2, 3 or 1, 3, 2). Although the theoretical foundations are the same in all cases, they result in different calculation formulations for the equations. The calculation of the principal axis angle φ_0 , is particularly problematic. As is the norm in technical mechanics, the principal axis angle lies between the x-axis and the principal strain ε_1 , or principal stress σ_1 in the mathematically positive direction of

rotation (counter-clockwise). While HBM has adopted this definition, from time to time, the angle is also offered by the y-axis in the mathematically negative direction. Further uncertainties result from the mathematical notations, such as \arctan or \tan^{-1} (equally valid for use in tangent function inversion) and also from the mixture of angle specifications, with angular degree (°) and radian measure (rad).

A uniform calculation concept is presented, starting from the mathematical foundations, to aid understanding of the evaluation of stress based on rosette measurements. The basis for this concept, which is described in the first part of this article, is that the principal axis angle only falls between 0° and +90° and between 0° and -90°. In the second part, evaluation equations are applied to determine the stress at several points of a stiffened, thin-walled regular cylinder under torsional stress. The design of this regular cylinder corresponds to the model of an aircraft fuselage. The findings are then checked by comparing them with the theoretical solution, which is also presented for the sake of completeness.

Determination of plain stress using strain gage rosettes

Siegmar Tittel, Dresden, Germany

Theory of rosette evaluation

To analyze the regularities of plain stress, a small triangular element of constant thickness h is cut out of a plane load-bearing structure (Fig. 1). The horizontal and vertical planes form an x/y coordinate system and the plane rotated around angle φ and its standard make up a uv coordinate system.

In accordance with the procedure represented by [1] and [2], the two force equilibrium equations follow in the u and v directions

$$\sum F_u = 0: \quad \sigma_u \cdot ds \cdot h - \sigma_x \cdot dy \cdot h \cdot \cos\varphi - \sigma_y \cdot dx \cdot h \cdot \sin\varphi - \tau_{xy} \cdot dy \cdot h \cdot \sin\varphi - \tau_{yx} \cdot dx \cdot h \cdot \cos\varphi = 0 \quad (1)$$

$$\sum F_v = 0: \quad \tau_{uv} \cdot ds \cdot h + \sigma_x \cdot dy \cdot h \cdot \sin\varphi - \sigma_y \cdot dx \cdot h \cdot \cos\varphi - \tau_{xy} \cdot dy \cdot h \cdot \cos\varphi + \tau_{yx} \cdot dx \cdot h \cdot \sin\varphi = 0 \quad (2)$$

from which are obtained the sectional stresses on the inclined plane:

$$\sigma_u = \frac{\sigma_x + \sigma_y}{2} + \frac{\sigma_x - \sigma_y}{2} \cdot \cos 2\varphi + \tau_{xy} \cdot \sin 2\varphi \quad (3)$$

$$\tau_{xy} = -\frac{\sigma_x - \sigma_y}{2} \cdot \sin 2\varphi + \tau_{xy} \cdot \cos 2\varphi \quad (4)$$

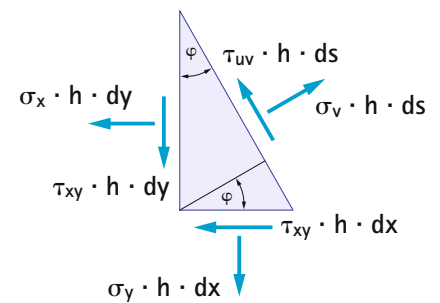


Fig. 1:
Forces at the triangular
element in the plain stress
state

At the sectional area $\varphi + \pi/2$ perpendicular to φ ,

$$\sigma_v = \frac{\sigma_x + \sigma_y}{2} - \frac{\sigma_x - \sigma_y}{2} \cdot \cos 2\varphi - \tau_{xy} \cdot \sin 2\varphi \quad (5)$$

The investigation now looks at the angles for which these stresses assume extremal values and how big these are. Standard stresses are extremal for $d\sigma_u/d\varphi = 0$ and for $d\sigma_v/d\varphi = 0$. Both these conditions produce the following equation:

$$\frac{d\sigma_u}{d\varphi} = 2 \cdot \left[-\frac{\sigma_x - \sigma_y}{2} \cdot \sin 2\varphi_0 + \tau_{xy} \cdot \cos 2\varphi_0 \right] = 0 \quad (6)$$

The direction of extreme standard stress (principal stress) is specified by the angle φ_0 .

$$\tan 2\varphi_0 = \frac{2 \cdot \tau_{xy}}{\sigma_x - \sigma_y} = \frac{\gamma_{xy}}{\epsilon_x - \epsilon_y} \quad (7)$$

The principal stresses σ_1 and σ_2 occurring under angle φ_0 and $\varphi_0 + \pi/2$ opposite the x-axis result in:

$$\sigma_1 = \frac{\sigma_x + \sigma_y}{2} + \frac{\sigma_x - \sigma_y}{2} \cdot \cos 2\varphi_0 + \tau_{xy} \cdot \sin 2\varphi_0 \quad (8)$$

$$\sigma_2 = \frac{\sigma_x + \sigma_y}{2} - \frac{\sigma_x - \sigma_y}{2} \cdot \cos 2\varphi_0 - \tau_{xy} \cdot \sin 2\varphi_0 \quad (9)$$

By using trigonometric addition theorems

$$\cos 2\varphi_0 = \frac{1}{\sqrt{1 + \tan^2 2\varphi_0}} = \frac{\sigma_x - \sigma_y}{\sqrt{(\sigma_x - \sigma_y)^2 + 4 \cdot \tau_{xy}^2}} \quad (10)$$

$$\sin 2\varphi_0 = \frac{\tan 2\varphi_0}{\sqrt{1 + \tan^2 2\varphi_0}} = \frac{2 \cdot \tau_{xy}}{\sqrt{(\sigma_x - \sigma_y)^2 + 4 \cdot \tau_{xy}^2}} \quad (11)$$

and by conversion, the principal stresses are obtained

$$\sigma_{1,2} = \frac{\sigma_x + \sigma_y}{2} \pm \sqrt{\left(\frac{\sigma_x - \sigma_y}{2}\right)^2 + \tau_{xy}^2} \quad (12)$$

From the condition $\frac{d\tau_{uv}}{d\varphi} = 0$, it follows that:

$$\tan 2\varphi_1 = -\frac{\sigma_x - \sigma_y}{2\tau_{xy}} \quad (13)$$

Determination of plain stress using strain gage rosettes

Siegmar Tittel, Dresden, Germany

Starting from principal stresses $\sigma_1 = \sigma_{\max}$ and $\sigma_2 = \sigma_{\min}$ the sectional stresses in an inclined plane under angle α work out at (Fig.2):

$$\sigma_u = \frac{\sigma_1 + \sigma_2}{2} + \frac{\sigma_1 - \sigma_2}{2} \cdot \cos 2\alpha \quad (14)$$

$$\tau_{uv} = -\frac{\sigma_1 - \sigma_2}{2} \cdot \sin 2\alpha \quad (15)$$

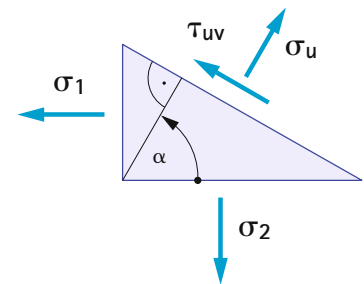


Fig. 2:
Sectional stresses at an inclined plane

If you regard α as the difference angle $\alpha = \varphi - \varphi_0$, where φ_0 is the angle between the principal stress plane standards and the x-axis and φ is the angle between the standards of the investigated plane and the x-axis, the sectional stresses turn out as:

$$\sigma_u = \frac{\sigma_1 + \sigma_2}{2} + \frac{\sigma_1 - \sigma_2}{2} \cdot \cos 2(\varphi_0 - \varphi) \quad (16)$$

$$\tau_{uv} = -\frac{\sigma_1 - \sigma_2}{2} \cdot \sin 2(\varphi_0 - \varphi) \quad (17)$$

As the principal strains behave in the same way as the principal stresses and the principle axis angle is the same, the following equations can be set up for SG rosettes.

$$\epsilon_a = \frac{\epsilon_1 + \epsilon_2}{2} + \frac{\epsilon_1 - \epsilon_2}{2} \cdot \cos 2(\alpha - \varphi_0) \quad (18)$$

$$\epsilon_b = \frac{\epsilon_1 + \epsilon_2}{2} + \frac{\epsilon_1 - \epsilon_2}{2} \cdot \cos 2(\beta - \varphi_0) \quad (19)$$

$$\epsilon_c = \frac{\epsilon_1 + \epsilon_2}{2} + \frac{\epsilon_1 - \epsilon_2}{2} \cdot \cos 2(\gamma - \varphi_0) \quad (20)$$

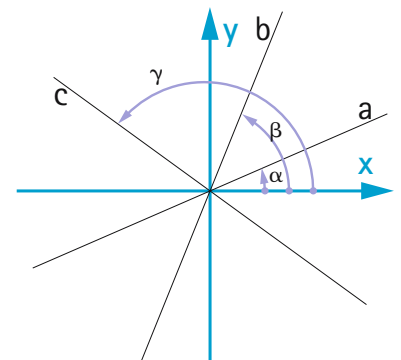


Fig. 3:
The angles of measurement directions a, b and c

This allows the evaluation equations shown below to be differentiated for the two usual rosette design types (0°, 60°, 120°) and (0°, 45°, 90°), with the distinction being made between three different cases, in accordance with the installation.

1st case:	45° rosette with	($\varepsilon_{-45}, \varepsilon_0, \varepsilon_{+45}$)	(-45°, 0°, +45°)
2nd case:	45° rosette with	($\varepsilon_0, \varepsilon_{+45}, \varepsilon_{+90}$)	(0°, +45°, +90°)
3rd case:	60° rosette with	($\varepsilon_{-60}, \varepsilon_0, \varepsilon_{+60}$)	(-60°, 0°, +60°)
4th case:	60° rosette with	($\varepsilon_0, \varepsilon_{+60}, \varepsilon_{+120}$)	(0°, +60°, +120°)

From the strains measured in the three directions, it is possible to use equations (21) – (36) specified below to calculate the required 9 target quantities $\varepsilon_1, \varepsilon_2, \varphi_0, \sigma_1, \sigma_2, \tau_{\max}, \sigma_x, \sigma_y, \tau_{xy}$

Principal strains

General solution:

$$\varepsilon_{1,2} = \frac{\varepsilon_{+\omega} + \varepsilon_{-\omega} - 2 \cdot \varepsilon_0 \cdot \cos 2\omega}{2 \cdot (1 - \cos 2\omega)} \pm \sqrt{\left(\frac{2 \cdot \varepsilon_0 - \varepsilon_{+\omega} - \varepsilon_{-\omega}}{2 \cdot (1 - \cos 2\omega)}\right)^2 + \left(\frac{\varepsilon_{+\omega} - \varepsilon_{-\omega}}{2 \cdot \sin 2\omega}\right)^2} \quad (21)$$

$$\tan \psi'' = \frac{\varepsilon_{+\omega} - \varepsilon_{-\omega}}{2 \cdot \varepsilon_0 - \varepsilon_{-\omega} - \varepsilon_{+\omega}} \cdot \tan(\omega) \quad (22)$$

1st case (45° rosette with -45°, 0°, +45°, $\omega = 45^\circ$)

$$\varepsilon_{1,2} = \frac{\varepsilon_{45} - \varepsilon_{-45}}{2} \pm \frac{\sqrt{2}}{2} \sqrt{(\varepsilon_{-45} - \varepsilon_0)^2 + (\varepsilon_0 - \varepsilon_{45})^2} \quad (23)$$

$$\tan \psi^\circ = \frac{\varepsilon_{45} - \varepsilon_{-45}}{2\varepsilon_0 - \varepsilon_{45} - \varepsilon_{-45}} = \frac{Z}{N} \quad (24)$$

2nd case (45° rosette with 0°, +45°, +90°, $\omega = 45^\circ$)

$$\varepsilon_{1,2} = \frac{\varepsilon_0 + \varepsilon_{90}}{2} \pm \frac{\sqrt{2}}{2} \sqrt{(\varepsilon_0 - \varepsilon_{45})^2 + (\varepsilon_{45} - \varepsilon_{90})^2} \quad (25)$$

$$\tan \psi^\circ = \frac{2\varepsilon_{45} - \varepsilon_0 - \varepsilon_{90}}{\varepsilon_0 - \varepsilon_{90}} = \frac{Z}{N} \quad (26)$$

3rd case (60° rosette with -60°, 0°, +60°, $\omega = 60^\circ$)

$$\varepsilon_{1,2} = \frac{1}{3}(\varepsilon_{-60} + \varepsilon_0 - \varepsilon_{+60}) \pm \frac{\sqrt{2}}{3} \sqrt{(\varepsilon_{-60} - \varepsilon_0)^2 + (\varepsilon_0 - \varepsilon_{+60})^2 + (\varepsilon_{+60} - \varepsilon_{-60})^2} \quad (27)$$

$$\tan \psi^\circ = \frac{(\varepsilon_{+60} - \varepsilon_{-60})\sqrt{3}}{2\varepsilon_0 - \varepsilon_{-60} - \varepsilon_{+60}} = \frac{Z}{N} \quad (28)$$

Determination of plain stress using strain gage rosettes

Siegmar Tittel, Dresden, Germany

4th case (60° rosette with 0°, 60°, 120°, $\omega = 60^\circ$)

$$\varepsilon_{1,2} = \frac{\varepsilon_0 + \varepsilon_{+60} + \varepsilon_{+120}}{3} \pm \frac{\sqrt{2}}{3} \sqrt{(\varepsilon_0 - \varepsilon_{+60})^2 + (\varepsilon_{+60} - \varepsilon_{+120})^2 + (\varepsilon_{+120} - \varepsilon_0)^2} \quad (29)$$

$$\tan \varphi^* = \frac{(\varepsilon_{+60} - \varepsilon_{+120}) \cdot \sqrt{3}}{2 \cdot \varepsilon_0 - \varepsilon_{+60} - \varepsilon_{+120}} = \frac{Z}{N} \quad (30)$$

Principal axis angle

Quadrant	Z	N	Angle φ_0	$\varphi^* = \text{Arctan}(\text{num}/\text{denom})$
I	+	+	$0^\circ \leq \varphi_0 \leq +45^\circ$	$\varphi_0 = \varphi^* / 2$
II	+	-	$+45^\circ \leq \varphi_0 \leq +90^\circ$	$\varphi_0 = (180^\circ + \varphi^*) / 2$
III	-	-	$-45^\circ \geq \varphi_0 \geq -90^\circ$	$\varphi_0 = (\varphi^* - 180^\circ) / 2$
IV	-	+	$0^\circ \geq \varphi_0 \geq -45^\circ$	$\varphi_0 = \varphi^* / 2$

Tab.1:
Determining the principal axis angle φ_0 , taking the sign of the numerator and the denominator into account in equations 24, 26, 28 and 30

Principal stresses

$$\sigma_1 = \frac{E}{1-\nu^2} (\varepsilon_1 + \nu \cdot \varepsilon_2) \quad (31)$$

$$\sigma_2 = \frac{E}{1-\nu^2} (\varepsilon_2 + \nu \cdot \varepsilon_1) \quad (32)$$

Maximum shear stress

$$\tau_{\max} = \frac{1}{2} (\sigma_1 - \sigma_2) \quad (33)$$

Stresses in the x-y system

$$\sigma_x = \frac{1}{2} (\sigma_1 + \sigma_2) + \frac{1}{2} (\sigma_1 - \sigma_2) \cos 2\varphi \quad (34)$$

$$\sigma_y = \frac{1}{2} (\sigma_1 + \sigma_2) - \frac{1}{2} (\sigma_1 - \sigma_2) \cos 2\varphi \quad (35)$$

$$\tau_{xy} = \frac{1}{2} (\sigma_1 - \sigma_2) \sin 2\varphi \quad (36)$$

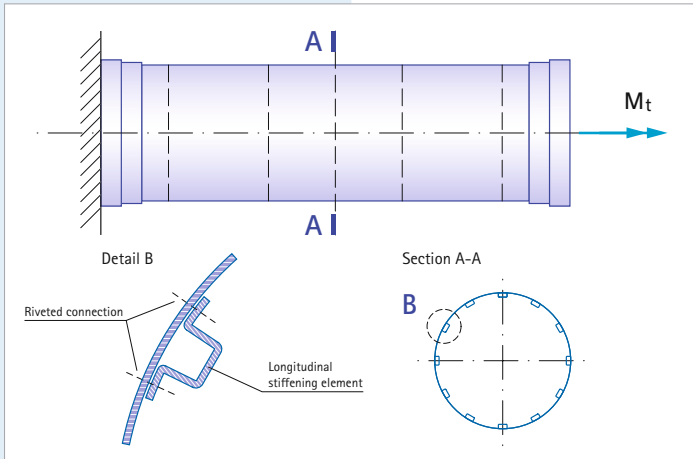


Fig. 4:
Stiffened shell of the regular cylinder, diagrammatic view

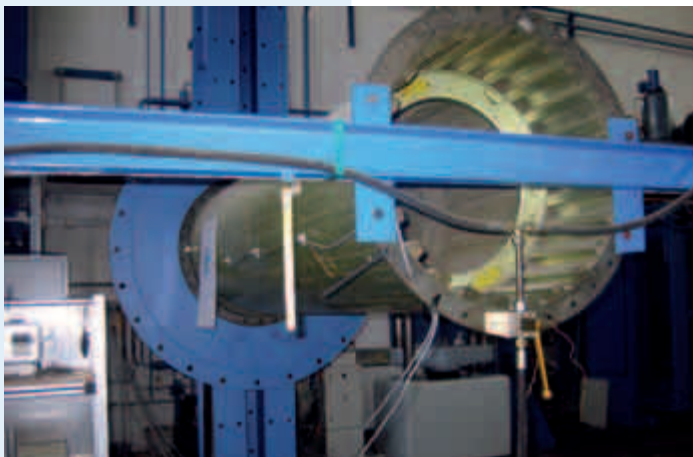


Fig. 5:
Test setup for experimental stress analysis

Stress analysis in the aircraft fuselage model

The accuracy of stress analysis with the relations shown is demonstrated by an example below. A stiffened regular cylinder shell made from AlCuMg, the basic design of which corresponds to a miniature model of an aircraft fuselage, is put under torsional stress. It is 2 m long and is stiffened longitudinally by 12 „top-hat” sections, spread evenly over the circumference. The number of „top-hat” sections is doubled to 24 at the ends for clamping and load application. Additional ring-shaped stiffening elements (frame sections) are fitted to increase stability. This torsion tube is loaded at the free protruding end by pure torsional moment. The regular cylinder shell is shown in diagrammatic form in Figure 4. Figure 5 shows the complete test setup.

The SG rosettes are used to measure the strains in the three fields and on a longitudinal section and the stresses will be determined from this. The longitudinal sections increase torsional stiffness, as they are riveted with the free sides at the skin. Bredt's formula is applied for the theoretical calculation of the stress distribution, that is to say, the torsional moment M_t that is introduced is absorbed by the complete tube and by the 12 part-tubes.

Theoretical determination of shear stresses

The cylinder is substantially stiffened by the 12 „top-hat” sections, with the shear flow at the riveted connections branching over the outer surface to the „top-hat” sections (Fig. 6) and the correlation to the loaded moment represented in equation 37 applies.

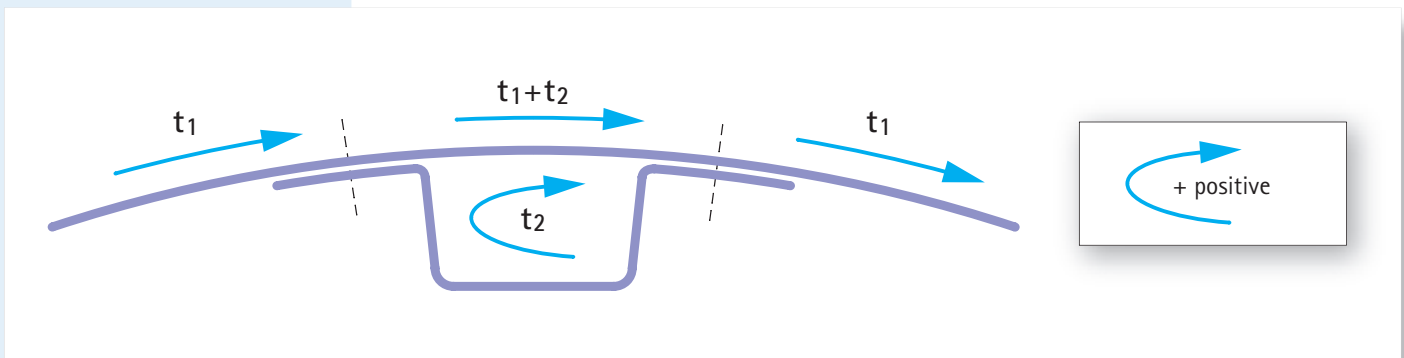


Fig. 6:
Distribution and direction of the shear flow

Determination of plain stress using strain gage rosettes

Siegmar Tittel, Dresden, Germany

$$Mt = 2 \cdot t_1 \cdot A_1 + 2 \cdot \sum t_2 \cdot A_2 \quad (37)$$

The torsional angle in the small tubes is identical to the torsional angle in the entire regular cylinder.

The torsional angle for a tube follows from:

$$\vartheta = \frac{1}{2 \cdot A} \cdot \oint \frac{t}{s \cdot G} du \quad (38)$$

whereby the following applies for the entire tube including the stiffening sections:

$$2 \cdot A \cdot \vartheta = t_1 \int_{11} \frac{du}{s \cdot G} + (t_1 + t_2) \cdot \sum_{12} \frac{du}{s \cdot G} \quad (39)$$

$$2 \cdot A \cdot \vartheta = t_2 \int_{22} \frac{du}{s \cdot G} + (t_2 + t_1) \cdot \sum_{12} \frac{du}{s \cdot G} \quad (40)$$

With displacement amounts δ

$$\delta_{11} = \int_{11} \frac{du}{s \cdot G} \quad ; \quad \delta_{12} = \int_{12} \frac{du}{s \cdot G} \quad ; \quad \delta_{22} = \int_{22} \frac{du}{s \cdot G} \quad (41)$$

you obtain the equational system (42) for the required quantities t_1 ; t_2 and ϑ

$$\begin{bmatrix} A_1 & \sum A_2 & 0 \\ (\delta_{11} + \sum \delta_{12}) & \sum \delta_{12} & -2 \cdot A_1 \\ \sum \delta_{12} & (\sum \delta_{22} + \sum \delta_{12}) & -2 \cdot \sum A_2 \end{bmatrix} \cdot \begin{bmatrix} t_1 \\ t_2 \\ \vartheta \end{bmatrix} = \begin{bmatrix} Mt/2 \\ 0 \\ 0 \end{bmatrix} \quad (42)$$

where $A_1 \dots$ is the cross-sectional area of the tube, $A_2 \dots$ is the stiffening section area, $\delta_{11} \dots$ is the displacement amount only with shear flow t_1 , $\delta_{12} \dots$ is the displacement amount with t_1 and t_2 , $\delta_{22} \dots$ is the displacement amount in the stiffening element section.

The shear stresses in the individual sections result from the shear flow and the wall thickness to:

$$\tau_{\text{Haut}} = \frac{t_1}{s} \quad \tau_{\text{Pröfil}} = \frac{t_2}{s} \quad \tau_{\text{Steg}} = \frac{t_1 + t_2}{s} \quad (43)$$

The distribution of the shear flow is shown in Figure 7.

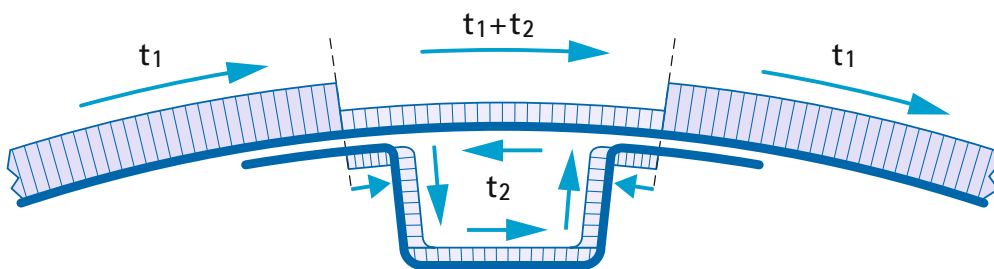


Fig. 7:
Shear flow in the outer surface and in the „top-hat“ section

For the experiment/theory comparison, the calculation of critical buckling shear stress according to

$$\tau_{krit} = 1,25 \cdot E \cdot \frac{s}{b} \cdot \sqrt{\frac{s}{r}} \quad (44)$$

is also required, as in the sub-critical range, when there is not yet any buckling, $\sigma_1 = -\sigma_2 = \tau$ applies. In equation 44, r represents the radius of the regular cylinder, s the thickness of the sheet in the skin of the cylinder and b the field width (distance between the rows of rivets). The shear stress and the shear flow can be determined experimentally from the strain values of the rosettes.

The calculation results for the load steps to be followed in the experiment are listed in Table 2.

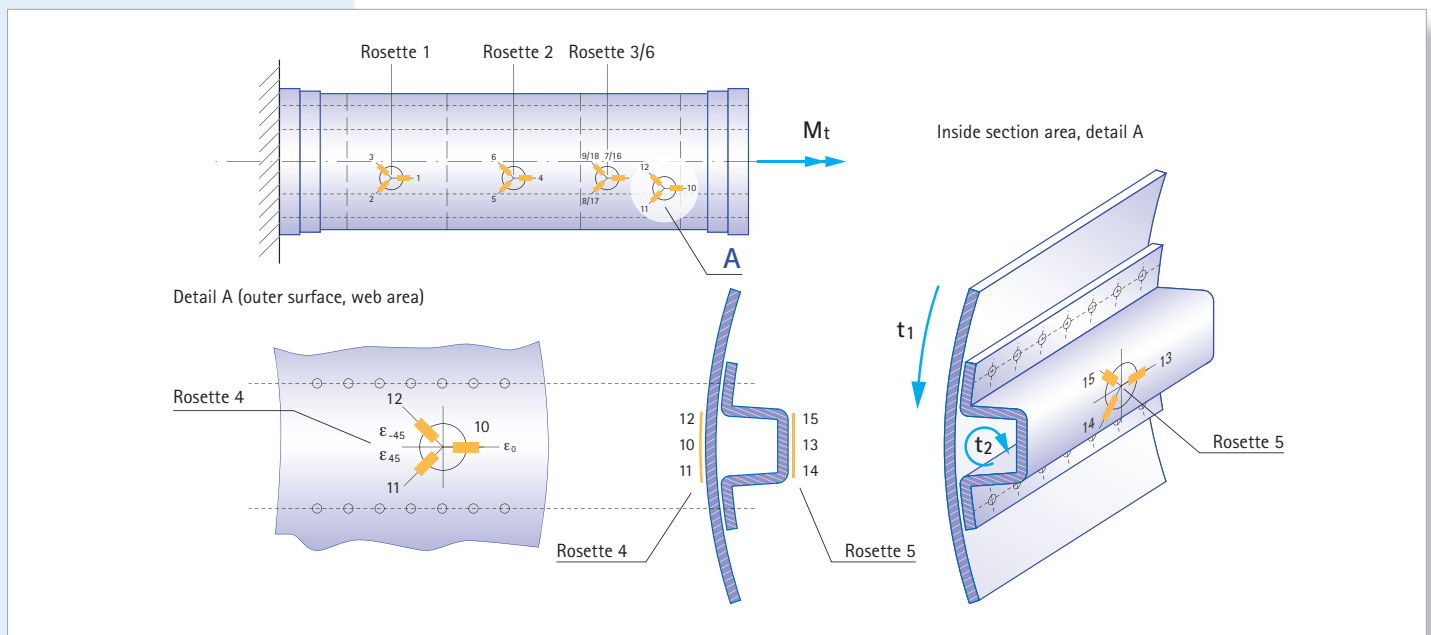
Tab. 2:
Theoretically calculated stresses

M_t [kN·m]	τ_{skin} [N/mm ²]	$\tau_{section}$ [N/mm ²]	τ_{web} [N/mm ²]
5	8.92	2.58	6.34
10	17.84	5.16	12.68
15	26.76	7.74	19.02
20	35.68	10.32	25.36

Fig. 8:
Positions of the SG rosettes on the shell of the cylinder

Experimental determination of shear stresses

For the experimental determination of the stresses, SG rosettes of the RY13-10/120 type (HBM) were installed at a total of 6 measuring points. The measured values were recorded with the UPM 100 multipoint measuring unit (HBM), in conjunction with a PC. The measuring point positions are shown in Figure 8. Rosettes 1-3 (SGs 1-9) are located on the outer surface



Determination of plain stress using strain gage rosettes

Siegmar Tittel, Dresden, Germany

between stiffening elements, rosette 4 (SGs 10-12) on the outer surface over a stiffening element, rosette 5 (SGs 13-15) on the inside at a stiffening element and rosette 6 (SGs 16-18) on the inside between stiffening elements. Figure 9 shows the test setup with the measuring device (on the left) and the SG rosettes. Table 3 (overleaf) contains the measured strain values of all the individual SGs in the four load steps.

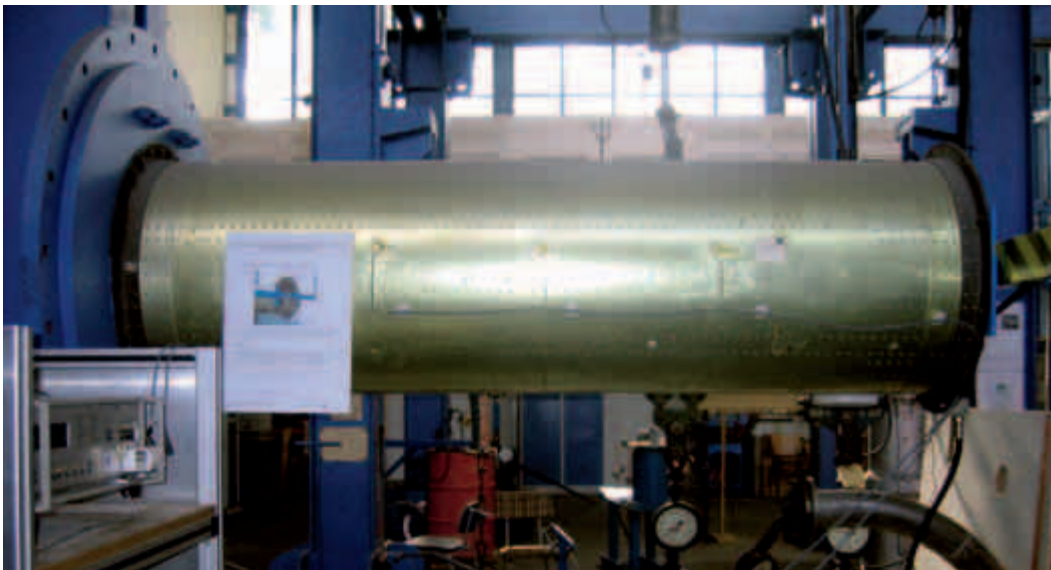
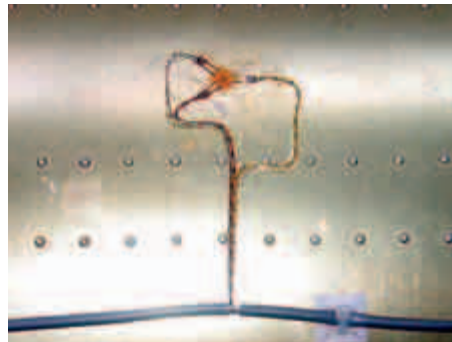


*Fig. 9:
Test setup with
installed HBM
SG rosettes
RY 13-10/120*



The principal stresses $\sigma_{1,2}$ and the principal stress angle φ_0 are calculated from these measured values. The angle is calculated in accordance with the frequently used elementary equation

$$\tan 2\varphi_0 = \frac{\epsilon_{45} - \epsilon_{-45}}{2\epsilon_0 - \epsilon_{45} - \epsilon_{-45}} \quad (45)$$

and in accordance with the improved equation (24), where a distinction is made between cases, in accordance with the signs of the numerator and the denominator of the tangent function, corresponding to Table 1. A direct comparison is made with the theoretical solution via the maximum shear stress. These results are combined in Table 4 (on page 13).

Rosette	SG	$M_t = 5 \text{ kN}\cdot\text{m}$	$M_t = 10 \text{ kN}\cdot\text{m}$	$M_t = 15 \text{ kN}\cdot\text{m}$	$M_t = 20 \text{ kN}\cdot\text{m}$
1	1	-5	0	0	0
	2	-150	-320	-440	-560
	3	170	320	470	650
2	4	-10	-15	-30	-50
	5	-174	-360	-525	-710
	6	150	320	456	620
3	7	0	20	25	45
	8	-164	-330	-485	-650
	9	170	330	480	690
4	10	-28	-80	-100	-110
	11	-140	-265	-400	-530
	12	130	230	340	420
5	13	0	0	-10	-30
	14	35	70	100	120
	15	-25	-50	-100	-130
6	16	45	80	90	95
	17	-175	-300	-480	-640
	18	208	380	550	690

Tab. 3:
Measured SG values
(strains in $\mu\text{m}/\text{m}$)

Estimating the results

The results presented in Table 4 indicate that the principal axis angle φ_0 produced in accordance with the elementary equation is incorrect for rosettes 1, 4 and 5 (printed in red). In the skin and in the web, the angle must have the same sign and theoretically assume the value of 45° . In the section, the shear flow works against the direction of the cylinder and so it also has a different sign. Correct values are always produced when, in accordance with equation 24, the sign of the numerator and the denominator are taken into account. In this example, it is not possible for different angles to be evaluated for the principal axes in the same shear field. It indicates rather more that when the elementary equation is applied for the principal axis angle, some of the angles that are defined are incorrect.

The theoretical calculation of the shear flows and the shear stresses is made under the assumption of ideal conditions. With

experimental stress analysis on the other hand, many influencing factors have a role to play, which results in the measured values deviating from the ideal values. The SG rosettes were applied under 45° , so that the 45° strip was in the horizontal direction (0°). Even slight differences to the prescribed angle cause errors. In the ideal case of pure torsion, strain must disappear at 0° . The two SGs under 45° and under -45° must have opposite signs but identical absolute values. If you look at Table 3 with the measured values, it is possible to identify vast differences. The following sources of error should be mentioned :

- Clamping and force application by a force couple was not exact.
- The riveting process caused the skin of the regular cylinder to prebuckle slightly.
- The SGs are not perfectly aligned.

Determination of plain stress using strain gage rosettes

Siegmar Tittel, Dresden, Germany

		Experiment					Theory	
Rosette	M_t [kN]	σ_1 [N/mm ²]	σ_2 [N/mm ²]	φ_0 in accordance with the elementary equation 45	φ_0 in accordance with equation 24 and Tab. 1	τ_{\max} [N/mm ²]	τ_{\max} [N/mm ²]	
1	5	9.6	-7.6	+42.3	-47.6	8.6	8.92	
	10	17.2	-17.2	+45.0	-45.0	17.2	17.84	
	15	26.0	-23.0	+44.0	-46.0	24.2	26.76	
	20	37.2	-28.2	+42.9	-47.1	32.7	35.68	
2	5	7.5	-9.9	-44.7	-44.6	8.7	8.92	
	10	16.3	-20.3	-44.6	-44.6	18.3	17.84	
	15	22.9	-29.8	-44.7	-44.7	26.4	26.76	
	20	31.9	-40.3	-44.8	-45.2	35.8	35.68	
3(6)	5	10.6	-8.7	-43.0	-43.0	9.7	8.92	
	10	20.1	-16.1	-42.4	-42.4	18.1	17.84	
	15	28.6	-25.3	-42.6	-42.6	26.9	26.76	
	20	38.3	-33.8	-43.0	-43.0	36.0	35.68	
4	5	6.9	-7.9	+40.2	-49.8	7.4	6.34	
	10	12.0	-15.5	+37.9	-52.1	13.7	12.68	
	15	17.3	-23.3	+39.6	-50.3	20.3	19.02	
	20	20.2	-31.2	+41.7	-48.3	25.7	25.36	
5	5	2.1	-1.1	-40.3	+49.7	1.6	2.58	
	10	4.2	-2.3	-40.3	+49.7	3.3	5.16	
	15	5.4	-5.4	-42.1	+47.8	5.4	7.74	
	20	6.4	-7.4	-39.3	+50.6	6.8	10.32	

In the sub-critical range, the measured strain values between rosettes 3 and 6 correspond well, which leads to the conclusion that the curved skin of the regular cylinder is so stiff, that it is sufficient to only take measurements at the outer contour. If, on the other hand, there is elastic buckling in the supercritical range, it is essential to measure both the inner and outer surface of the skin congruently. If the design makes it impossible to get at the inside to take measurements, then the curvature must be determined by an alternative method of measurement at the outer contour.

It is finally worth noting that with thin-walled structures, there are always differences between the results of experimental stress analysis using strain gages and the theoretical calculation. However, the results can be rated as good.

References

- [1] Göldner/Holzweißig: Leitfaden der Technischen Mechanik, Fachbuchverlag, 1980.
- [2] Schnell/Gross/Hauger: Technische Mechanik 2 – Elastostatik, Springer-Verlag, 1992

Tab. 4:
Comparison of rosette
evaluation results
(experiment) and
theoretically calculated
values (theory)



ram reports in applied measurement

Experimental analysis of mechanical stress in passive reinforcement anchorages in C-C-T nodes

C. Castro, P. Miguel,
M. A. Fernández, J. R. Martí,
Polytechnic University
of Valencia, Spain

Summary

The article presents a new test for analyzing the mechanical stress of adhesion anchors in C-C-T nodes. The primary aim of the investigation is to develop a practical design standard which, in the form of a dimensioning program, can be used to define important parameters for reinforcement anchorages. As well as the various concrete qualities and bar diameters, the parameters used in the program include the adhesion length and the angle of inclination of the tie bar. Described below are the construction and instrumentation of the test piece, the test setup, the way in which the experiments were performed and the results.

Introduction

When designing concrete structures, the precise dimensioning of the anchorages is a difficult problem, that can only be solved on the basis of experimental and theoretical investigations. Important aspects of this problem are dealt with in reference items [1]–[14]. Of particular significance is the interpretation of the geometric dimensions such as the length of the anchorage in elements such as brackets, moldings or structural elements supported by girders. The strength of adhesion depends not only on the length of the anchorage, but also the

compression parameters of the concrete. High transverse compressions (perpendicular to the reinforcement bar) vastly improve the strength properties, thus allowing the length of the anchorage to be reduced. To quantify this correlation, a new test was developed which allows the adhesion forces of CCT nodes (compression-compression-tension joints) to be analyzed and the application of tensile stress to the reinforcement bar to be recorded metrologically. A distinction is made between the load amounts transmitted to the transverse compression area of the concrete and those diverted into the reinforcement bar of the anchorage. The aim of the investigation is the development and experimental support of a dimensioning program that allows the construction engineer to specify reinforcement anchors in CCT nodes. The available parameters in this program are the concrete quality, the diameter of the reinforcement bar, the application length at the reinforcement bar (adhesion length) and the angle of inclination of the bar axis to the flow of force. To determine the transmission of force to the reinforcement bar, the investigation looks at the distribution of force to the concrete structural element and the bar, when the force is introduced obliquely into the bond. The diagram in Figure 1 clarifies the flow of force in the concrete.

Experimental analysis of mechanical stress in passive reinforcement anchorages in C-C-T nodes
 C. Castro, P. Miguel, M. A. Fernández, J. R. Martí, Polytechnic University of Valencia, Spain

The horizontal component of force C applied obliquely under angle θ is split into amount T_1 (transmitted by the joint) and amount T_2 (absorbed by the anchor). The vertical component is supported as amount R by the lower bearing.

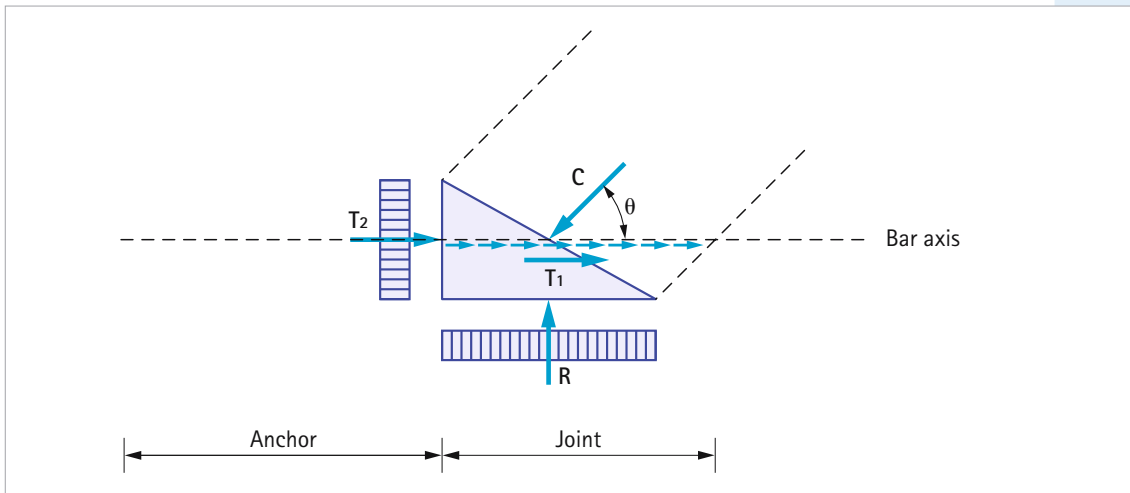


Fig. 1:
 Diagrammatic
 view of force
 distribution in
 concrete

The total bar force, produced from the force equilibrium in the horizontal direction, is

$$T = T_1 + T_2 = C \cdot \cos \theta \quad (1)$$

with amount T_1 , as shown in Figure 2, being applied gradually to the bar over the length of the joint.

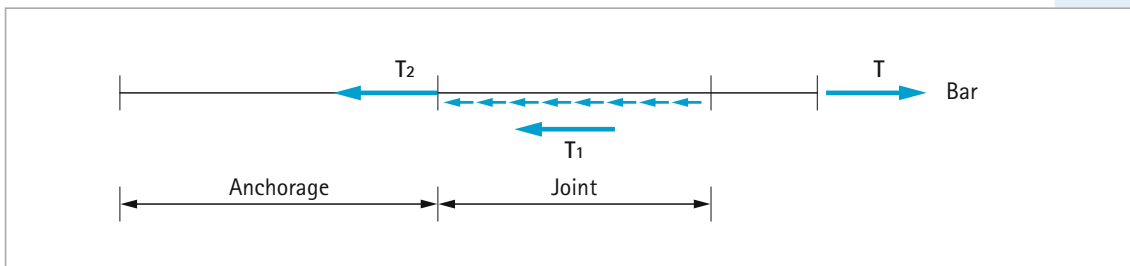


Fig. 2:
 Diagrammatic
 view of the
 longitudinal force
 response in the
 reinforcement bar

Experimental analysis of mechanical stress in passive reinforcement anchorages in C-C-T nodes

C. Castro, P. Miguel, M. A. Fernández, J. R. Martí, Polytechnic University of Valencia, Spain

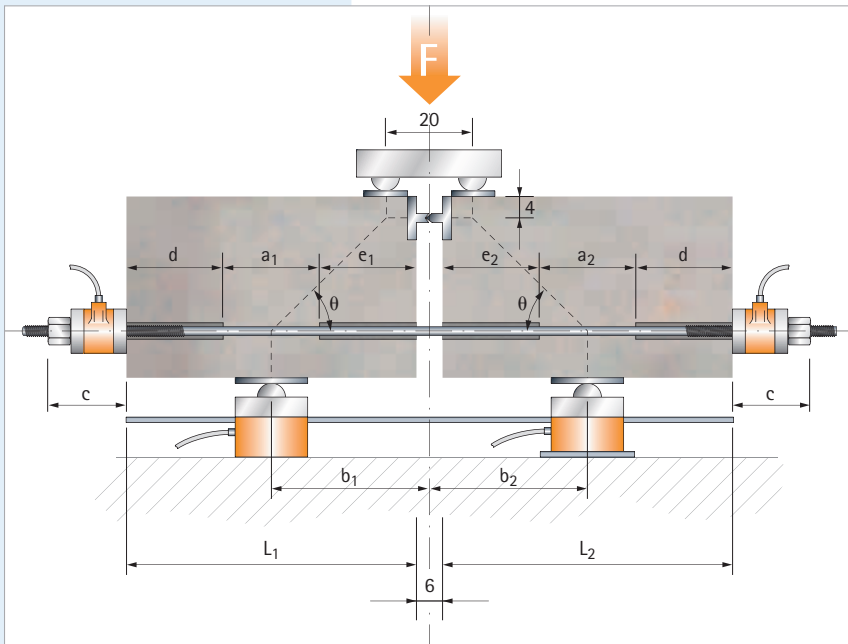


Fig. 3:
Test piece with loading



Fig. 4:
Test piece with
loading device

Test facility

The experimental implementation of the stress ratios presented in Figure 1 is achieved by using a concrete test piece that is split in two, with both the parts connected by a reinforcement bar with a solid reinforcement anchorage (Fig. 3).

While the cross-sectional measurements are fixed, with a width of 15 cm and a height of 24 cm, various dimensions such as the adhesion lengths, a_1 and a_2 , are variable, so that tests can be run with different parameters, such as the angles of inclination. The solid joint between the reinforcement bar and the concrete is only made in the exactly prescribed areas in both the parts. In areas d and e , adhesion is prevented by inserting PVC sleeves. The reinforcement bar is anchored at the outside ends of the blocks, by a nut and a washer in each case. Force transducers are fitted here to measure the residual anchoring force (Fig. 5). Steel elements are added in the upper block area to transmit the compressive forces that arise between the blocks when under load. These implement a flexible joint with sharp edges and fins.

To perform the test, this test piece is fitted into a hydraulic load frame (1,000 kN), where it is supported underneath on two free-moving rollers lubricated with MoS₂ graphite mounting paste. At the top, total force F is distributed by a bridge and is introduced to the test piece also via cylindrical rollers. All the force application points to the concrete are strengthened by inserting steel plates. Figure 4 shows the test piece fitted into the load frame.

Experimental analysis of mechanical stress in passive reinforcement anchorages in C-C-T nodes

C. Castro, P. Miguel, M. A. Fernández, J. R. Martí, Polytechnic University of Valencia, Spain

Receiving and processing measured values

During the continuous loading of the sample generated by the hydraulic test machine, the following mechanical quantities are recorded metrologically.

1. Forces

- Total force of the hydraulic cylinder
- Bearing forces at the lower supports
- Anchoring forces at the side anchorages of the reinforcement bar.

Various HBM force transducers, such as the C6A (200 kN) and the C2 (100 kN) were used to measure force. As an example, Figure 5 shows the C6A force transducer (200 kN) that was used to measure the anchoring forces.

2. Strains

- Strains in three directions (rosette measurement) in the force flow area of the concrete blocks, with LY42-50/120 strain gages (HBM) (Fig. 6a, measuring points 1 to 6)
- Longitudinal strain in the center of the reinforcement bar, with LY41-3/120 strain gages (HBM), to determine bar force T (Fig. 6a, measuring points 7 and 8 and Fig. 7)

3. Displacements

- Opening of the central gap between the concrete blocks, with SLS190/50 displacement transducers (Penny+Giles) (Fig. 6a, measuring points 15 and 16)



Fig. 5: C6A 200 kN force transducer for measuring external anchoring forces

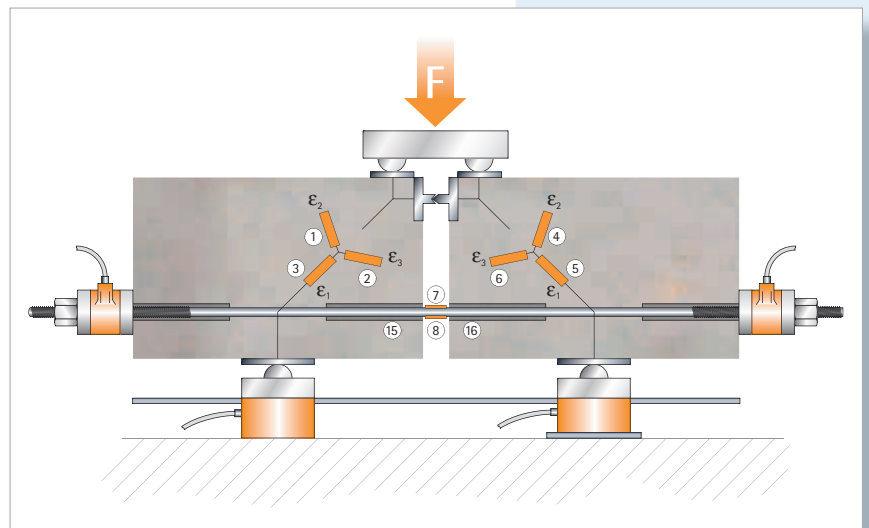


Fig. 6a: Position of the SGs and the displacement transducers: 1-6 LY42-50/120 SGs (HBM), 7-8 LY41-3/120 SGs (HBM), 15-16 displacement transducers



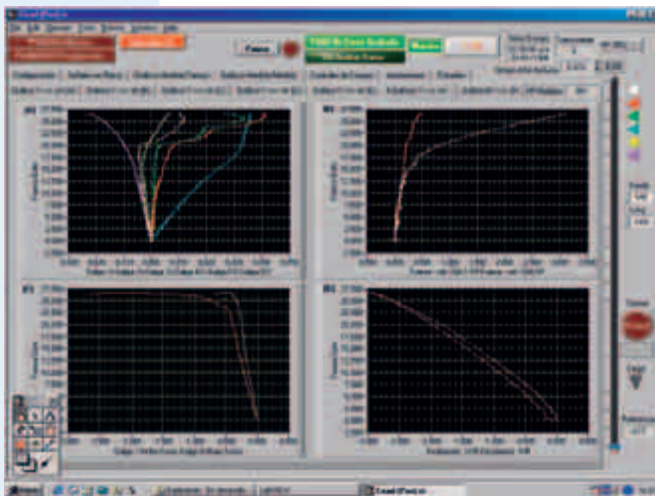
Fig. 6b: View of the complete installation

Experimental analysis of mechanical stress in passive reinforcement anchorages in C-C-T nodes
 C. Castro, P. Miguel, M. A. Fernández, J. R. Martí, Polytechnic University of Valencia, Spain

Fig. 7:
 LY41-3/120
 SGs (HBM) for
 measuring total
 bar force T



Fig. 8:
 Display of
 measured
 values in real
 time during the
 test run



A software package program developed at the Civil Engineering Institute of the Polytechnic University of Valencia was used for automatic control of the test machine and to record, visualize and store all the data in real time. Figure 8 shows the real-time presentation of the measured values during a test run. All the measured values are represented as a function of the total force. The details are as follows: top left are the strain values of measuring points 1 - 6; bottom left is the total bar force, calculated from the strain values of measuring points 7 and 8; top right are the anchoring forces at the external fastening points and bottom right are the displacements at measuring points 15 and 16.

Test program and results

A total of 81 instrumented test pieces were tested in the described test facility. The tests differed with regard to concrete quality, execution and inclination of the reinforcement anchor and adhesion length. The test parameters are listed in Table 1.

The parameters were used as the name to uniquely identify the sample and the test. Thus, for example, (V-25/16/45/10-25) means concrete strength 25MPa, bar diameter 16mm, angle of inclination 45° and adhesion lengths 10cm on the left and 25cm on the right side of the test piece. The correlation measured at this test piece

Tab. 1:
 Parameters of
 the test pieces
 used

Parameters	Value		
Concrete quality (compressive strength in MPa)	25	50	80
Diameter of the reinforcement anchor in mm	12	16	20
Angle of inclination of the anchor to the flow of force in °	27	45	63
Adhesion length (left to right) in cm	5 - 20	15 - 15	10 - 25

Experimental analysis of mechanical stress in passive reinforcement anchorages in C-C-T nodes

C. Castro, P. Miguel, M. A. Fernández, J. R. Martí, Polytechnic University of Valencia, Spain

between the total tensile force T , measured in the tie bar and the anchoring force T_2 recorded at the external anchorage point is shown in the graph in Figure 9 (equation 1 and Fig. 2).

This clearly shows that with an adhesion length of $a = 10$ cm, the total force is transmitted virtually totally to the concrete block via the bond, up to a value of $T \approx 60$ kN, which corresponds to a longitudinal stress of $\sigma = 300$ MPa. The external residual anchoring force stays very small, at $T_2 \approx 2$ kN in this initial area. There is then a more pronounced increase in T_2 and at $T \approx 100$ kN, a value of $T_2 \approx 13$ kN is reached. In this load range, adhesion subsides increasingly between 60 kN and 100 kN, with the maximum force that can be transmitted by the bond being $T_1 = T - T_2 = 87$ kN. Any further increase in load will lead to the failure of the tie bar. If the adhesion length is $a = 25$ cm, it is not possible to observe any subsidence in adhesion until $T \approx 100$ kN. The joint will also fail here if the maximum load in the tie bar is exceeded.

As well the failure of the tie bar as a result of exceeding the maximum endurable tensile stress, the tests made it possible to observe a further failure mechanism. This is a crack that divides the concrete solid vertically into two pieces, before the tie bar fails (Fig. 10).

In Figure 10, the area marked by (a) on the exposed tie bar is that in which a joint between the concrete and the tie bar is prevented by the PVC sleeves. The actual adhesion area is identified by (b) and (c) marks the SGs that were used to measure the total anchoring force T .

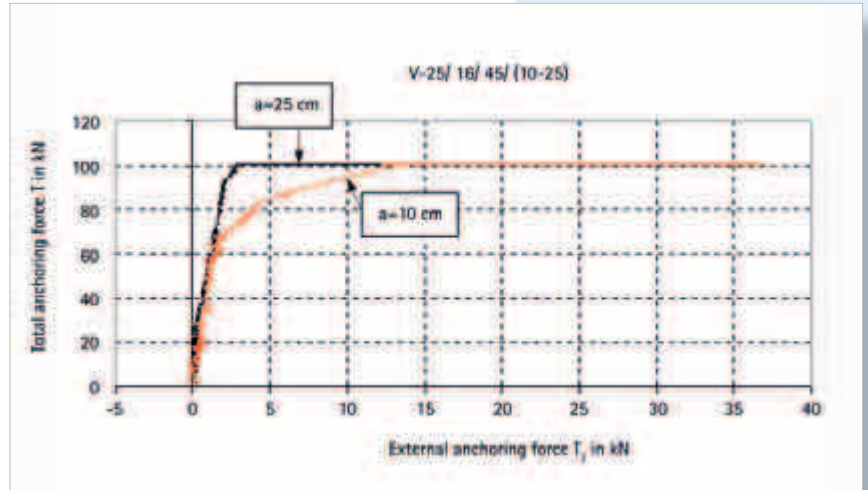


Fig. 9: Correlation between total anchoring force T and external anchoring force T_2 for adhesion lengths $a = 10$ cm and $a = 25$ cm

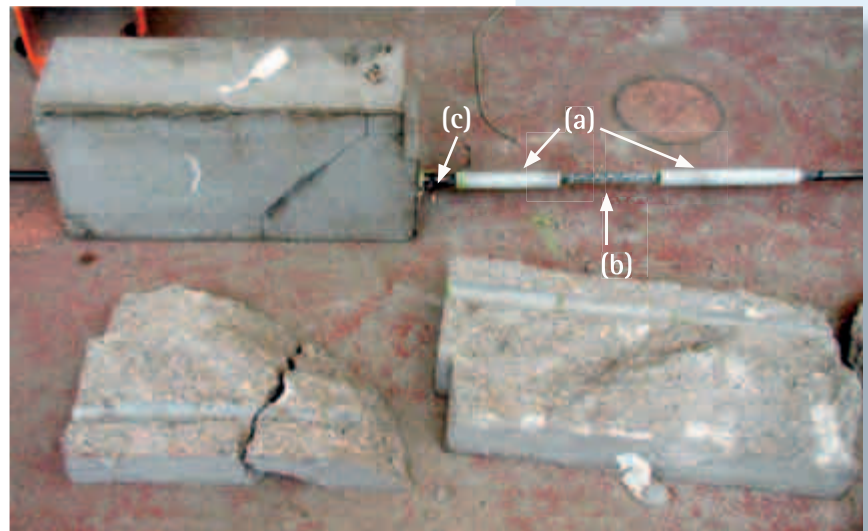


Fig. 10: Joint failure caused by cracks forming

Experimental analysis of mechanical stress in passive reinforcement anchorages in C-C-T nodes

C. Castro, P. Miguel, M. A. Fernández, J. R. Martí, Polytechnic University of Valencia, Spain

Conclusions

Compared to other, well-known tests, the test procedure described here has the advantage that the transverse load increases in proportion to the tensile force in the reinforcement bar, so that the angle of inclination between the forces remains constant while the load is increasing. This enables the stress simulated in the test to correspond very well to the actual ratios, as they occur in real life in the anchorages of girders, brackets or moldings. The idea of having a test piece that is split in two enables two tests to be carried out simultaneously with different parameters, with it always being possible to run the tests to their conclusion until failure, for both sides, even if the joint on one side gives way prematurely. In previous test implementations, the maximum load was limited both by the tie bar giving way and by cracks forming.

Because of the extensive instrumentation and the fact that the measured values are recorded in real time, the state of the joint can be watched continually. Because the strain gages are prepared at the outer surfaces of the concrete blocks in the force flow area, incipient cracks can be detected in good time by increasing the strain. The important strength properties of the joint can be assessed, with precise force measurement, especially of the force transmitted from the tie bar to the concrete block and thus the requisite adhesion length, making it possible to accurately determine the adhesion length.

References

- [1] ADEBAR P., KUCKMA D. and COLLINS M.: Strut-and-Tie Models for Design of Pile Caps: An Experimental Study, *ACI Structural Journal*. V. 87. No 1. Jan-Feb. 1990.
- [2] BRIAN S. MAXWELL, JOHN E. BREEN.: Experimental Evaluation of Strut-And-Tie Model Applied to Deep Beam with Opening, *ACI Structural Journal*, Jan-Feb, 2000.
- [3] Code Model. CEB-FIP 1990.
- [4] E.H.E. INSTRUCCIÓN DE HORMIGÓN ESTRUCTURAL, Ministerio de Fomento.
- [5] HONG S-G.: Truss Model for Tension Bars in Reinforced Concrete Beams: Tension-Tension-Compression Regions, *ACI Structural Journal*. V. 93. No 6. Nov-Dec. 1996.
- [6] HONG S-G.: Strut-and-Tie Models and Failure Mechanisms for Bar Development in Tension-Tension-Compression Nodal Zone, *ACI Structural Journal*. V. 97. No 1. Jan-Feb. 2000.
- [7] HONG S-G., MUELLER P.: Truss Model and Failure Mechanism for Bar Development In C-C-T Nodes, *ACI Structural Journal* V. 93. No. 5 Sept-Oct, 1996.
- [8] JOHANSSON M.: Nonlinear Finite-Element Analysis of Concrete Frame Corners, *Journal of Structural Engineering*. Jan-Feb. 2000.
- [9] LIANG Q.Q., XIE Y.M. and STEVEN G.P.: Optimal Topology Selection of Continuum Structures with Displacement Constraints, *Computers and Structures* 77. Pergamon 2000.
- [10] MARTÍNEZ, MARTÍNEZ, A.: Sistematización Numérica del Método Biela – Tirante, Final Project in E.T.S.I.C.C.P. of Valencia (Spain). Professor: Pedro F. Miguel Sosa. U.P.V.1998.
- [11] SCHLAICH J., SCHÄFER K, JENNEWEIN M.: Toward a Consistent Design of Structural Concrete, *PCI Journal*, V.32. No. 3, May-Jun, 1987.
- [12] SCHLAICH M., ANAGNOSTOU G.: Stress Fields for Nodes of Strut and Tie Models, *Journal of Structural Engineering*, Jan 1990.
- [13] SIAO W.B.: Shear Strength of Short Reinforced Concrete Walls, Corbels and Deep Beams, *ACI Structural Journal*. V. 91. No 2 Mar-Apr. 1994.
- [14] YUN Y.M. and RAMÍREZ J.A.: Strength of Struts and Nodes in Strut Tie Models, *Journal of Structural Engineering*. Vol 122. No. 1. 1996.

ram

You are invited to contribute an article or articles to ram, and will receive an author's fee if your article is published.

Contact:

E-mail, editor: Martin.Stockmann@Mb.TU-Chemnitz.de

E-mail, HBM: klaus.bathe@hbm.com

Reply fax to the editor: +49 (0) 371 5311471

Name _____

Company / Dept. _____

Street _____

Town, Postal code _____

Telephone _____

Fax _____



I am interested in having an article published in ram and would ask you to kindly contact me

imprint

Published by:

Hottinger Baldwin Messtechnik GmbH
Im Tiefen See 45
D-64293 Darmstadt
Tel. +49 6151 803-0
Fax +49 6151 803-9100
www.hbm.com

Editor

Dr.-Ing. habil. Martin Stockmann
Chemnitz University of Technology

Please address any questions about ram articles to the publisher.

Please address any questions about HBM products to your local HBM sales office.

Copyright

Copying is only permitted with the advance written approval of the editorial office or the publisher. Copying or reproduction in the form of photocopies, microfilm or other means for commercial purposes is not permitted.

All rights reserved

No liability can be accepted for the procedures and circuits described and the names used in respect of the infringement of patents or trademarks of third parties.

Design & Artwork

www.contrust-design.de

reports in applied measurement 2/2005

Issued: December 2005

"reports in applied measurement" is issued twice annually

ISSN 1614-9912



measurement with confidence

Hottinger Baldwin Messtechnik GmbH

Im Tiefen See 45
64293 Darmstadt
Germany

Tel. +49 (0) 6151 80-30
Fax +49 (0) 6151 803-9100

E-mail: info@hbm.com
Internet: www.hbm.com